Detection and Imaging of Superoxide in Roots by an Electron Spin Resonance Spin-Probe Method

Nasim Warwar,[†] Avishai Mor,[‡] Robert Fluhr,[‡] Ramasamy P. Pandian,[§] Periannan Kuppusamy,[§] and Aharon Blank[†*]

[†]Schulich Faculty of Chemistry Technion, Israel Institute of Technology, Haifa, Israel; [‡]Department of Plant Sciences, Weizmann Institute of Science, Rehovot, Israel; and [§]Center for Biomedical EPR Spectroscopy and Imaging, Davis Heart and Lung Research Institute, Department of Internal Medicine, The Ohio State University, Columbus, Ohio

ABSTRACT The detection, quantification, and imaging of short-lived reactive oxygen species, such as superoxide, in live biological specimens have always been challenging and controversial. Fluorescence-based methods are nonspecific, and electron spin resonance (ESR) spin-trapping methods require high probe concentrations and lack the capability for sufficient image resolution. In this work, a novel (to our knowledge), sensitive, small ESR imaging resonator was used together with a stable spin probe that specifically reacts with superoxide with a high reaction rate constant. This ESR spin-probe-based methodology was used to examine superoxide generated in a plant root as a result of an apical leaf injury. The results show that the spin probe rapidly permeated the plant's extracellular space. Upon injury of the plant tissue, superoxide was produced and the ESR signal decreased rapidly in the injured parts as well as in the distal part of the root. This is attributed to superoxide production and thus provides a means of quantifying the level of superoxide in the plant. The spin probe's narrow single-line ESR spectrum, together with the sensitive imaging resonator, facilitates the quantitative measurement of superoxide in small biological samples, such as the plant's root, as well as one-dimensional imaging along the length of the root. This type of methodology can be used to resolve many questions involving the production of apoplastic superoxide in plant biology.

INTRODUCTION

Superoxide anion radical, $O_2^{\bullet -}$, is an important member of the reactive oxygen species (ROS) class. Under normal conditions, it is generated in cells as a byproduct of mitochondrial respiration. In plants, it may also be formed in the chloroplasts during photosynthesis. In addition to being a byproduct of metabolism, superoxide has a wide variety of functions and effects in stress biology. For example, it is used by the immune system to kill invading microorganisms, and it plays an important role in signaling by activating metabolic pathways and controlling growth (1–3). Superoxide radicals also appear in response to pathogen and wound stresses (4–7). The formation of ROS in a cellular context may be destructive in terms of membrane integrity, DNA damage, and protein homeostasis. Therefore, cells employ efficient scavenging systems to control the levels of ROS during normal metabolism as well as in response to different stresses (8).

In view of the importance of superoxide, investigators have made many efforts to develop reliable and useful methods for accurate detection and imaging of this species in its biological arena. Because of its low steady-state concentration (~10^{-10} M (9)) and short lifetime, as well as the presence of competing intra- and extracellular oxidants and enzymes, such as superoxide dismutases (SOD), it is challenging to measure superoxide levels. Several publications have reviewed many of these methods (10–13), and it is important to appreciate the scope of use and limitations of each approach, as briefly summarized below:

1. A common method to evaluate superoxide levels inside cells is to look at the ratio of active to inactive aconitase, because superoxide inactivates this enzyme by fast reaction (9). The method makes assumptions about the superoxide-aconitase second-order reaction rate constant and the constant activation rate. Because of these and other difficulties, the method can only provide a rough estimate of the total superoxide levels in the cell (10,11). The method does not involve any exogenous probe, but requires cell harvesting and thus lacks any time-resolved and imaging capabilities (10,11). Other methods that can perform imaging in a time-resolve manner make use of exogenous probes and can be divided into several groups according to the basic physical principle of detection.
2. Chemiluminescent detection relies on light being generated by reactions of exogenous molecular probes and superoxide. For example, lucigenin (bis-N-methylacridinium) is used for luminescent detection of the superoxide radical by means of a xanthine oxidase/hypoxanthine (XO/HX) system or by activated phagocytes (10). However, the lucigenin monocation radical has been shown to autoxidize and produce superoxide in the absence of $O_2^{\bullet -}$ (11). Luminol, another chemiluminescent reporter, must be univalently oxidized to the luminol radical, which reacts with $O_2^{\bullet -}$ emitting light. However, the luminol radical can spontaneously reduce O_2 to $O_2^{\bullet -}$ (11). Other compounds that have been used for chemiluminescent detection of $O_2^{\bullet -}$ but display similar limitations include

Submitted May 17, 2011, and accepted for publication July 22, 2011.

*Correspondence: ab359@tx.technion.ac.il

Editor: Betty J. Gaffney.

0006-3495/11/09/1529/10 $2.00

doi: 10.1016/j.bpj.2011.07.029

coelenterazine (2-(4-hydroxybenzyl)-6-(4-hydroxyphenyl)-8-benzyl-3,7-dihydroimidazo [1,2a]pyrazin-3-one) and its analogs CLA (2-methyl-6-phenyl-3,7-dihydroimidazo [1,2-a]pyrazin-3-one) and MCLA (2-methyl-6-(4-methoxyphenyl)-3,7-dihydroimidazo[1,2-a]pyrazin-3-one) (10).

3. Spectrophotometric probes are also used for superoxide detection. For example, nitroblue tetrazolium (NBT) can be reduced by superoxide to the purple/blue formazan precipitate (10,13–15). However, spectrophotometric methods lack sensitivity, and the NBT radical intermediate can also react with molecular oxygen under aerobic conditions and generate $O_2^{\bullet-}$ artificially, which can further reduce the NBT (10).
4. Fluorescence techniques make use of probes, such as hydroethidine, that can be oxidized by two superoxide molecules to generate fluorescent ethidium (12,16). However, hydroethidine is also oxidized by cytochrome *c* and H_2O_2, and high hydroethidine concentrations can lead to a spurious increase in fluorescence signal independently of $O_2^{\bullet-}$ or to an increase of the O_2^- dismutation rate to H_2O_2 (12). Superoxide anions can also react with nonfluorescent 2-(2-pyridil)-benzothiazoline and create a highly fluorescent product, 2-(2-pyridil)-benzothiazol. One of the limitations of this methodology is that it must be generated under alkaline conditions and thus has limited biological use (12). In a recent development, a genetically encoded superoxide reporter was used for intracellular measurements of superoxide (17). However, this method necessitates the generation of transgenic plants or animals and so far has been used only in animal cells. It can be concluded that the availability of fluorescence probes, combined with a relatively easy-to-use and accessible imaging modality, has made this a popular method; however, as noted above, there are major concerns associated with the specificity and quantitative aspects of these measurements (12,16). As a result, it is clear that fluorescence-based methods allow one to draw only semiquantitative conclusions about the effects of various treatments or pathological conditions on intracellular steady-state levels (or flux) of superoxide radicals by comparing the amount of fluorescence signals in different treatments.
5. ESR can take advantage of the superoxide's paramagnetic state; however, the low steady-state concentration, short lifetime, and large rotational angular momentum component of this small diatomic molecule prevent it from being detected directly by ESR. A common method to overcome this difficulty is based on the use of spin traps, which are diamagnetic molecules that, upon reaction with a superoxide, generate relatively stable paramagnetic species (18). Examples of common spin traps include DMPO (5,5-dimethyl-1-pyrroline-*N*-oxide) and a more recent derivative of this trap, BMPO (5-*tert*-butoxycarbonyl 5-methyl-1-pyrroline *N*-oxide), which reacts with the superoxide to create a relatively stable (in the tens-of-minutes range) spin adduct (19). This method is specific because the adduct spectrum is different for different trapped ROS. However, it suffers from several disadvantages: Large concentrations (>10 mM) must be used to obtain enough signal and compete with other processes, and the reaction may not be specific, as different ROS can react with the same trap, leading to spectral overlap. Another severe limitation is the lack of a high-resolution imaging modality that makes use of this methodology to pinpoint the exact location of superoxide creation. This is due to instrumental limitations and the broad, complex, multiline ESR spectrum of spin traps that make imaging very challenging (i.e., requiring larger gradients and suffering from artifacts due to the multiplicity of lines in the spectrum). Nonetheless, a lot of work has been done with spin traps. For example, the tiron spin trap (4,5-dihydroxy-1,3-benzenedisulfonic acid disodium salt) was used in botanical research to measure superoxides in injured roots (20). In addition, ESR studies on hydroxyl radicals in cucumber roots and *Arabidopsis* seedlings yielded a general localization of this ROS species (21). A combined ESR/fluorescence probe was also used for in vitro applications (22).

In this work we present a less common methodology for the detection of superoxides in biological samples. Our approach is based on ESR, but instead of making use of spin traps, we work with a paramagnetic spin probe, perchlorotriphenylmethyl radical-tricarboxylic acid (PTM-TC) (Fig. 1 *a*) (23). The spin probe method works in a somewhat opposite manner to spin trapping. A relatively stable paramagnetic spin probe reacts with free radicals and becomes diamagnetic. A loss of signal is indicative of the presence of ROS. This method has been demonstrated with a variety of spin probes, such as nitroxides (24,25), but presented specificity problems similar to those mentioned above. The probe employed in this study is water-soluble but not cell-permeable. It was found to react very specifically with superoxide and become diamagnetic with a very high second-order

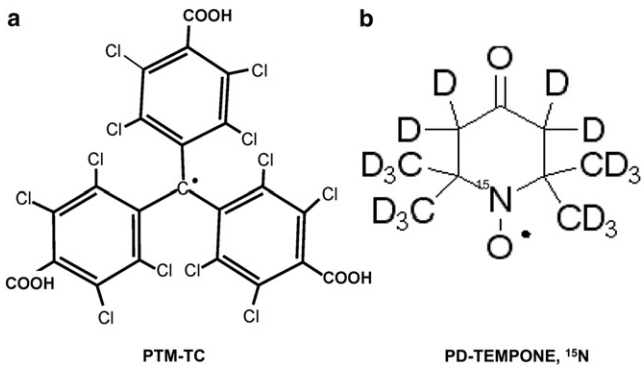

FIGURE 1 Chemical structure of the stable free radicals employed in this work.

reaction rate constant of 8.3×10^8 $M^{-1}s^{-1}$. On the other hand, in vitro tests showed that other common free radical species, such as OH, $ROO^{\cdot}$, H_2O_2, NO, GSH, and L-ascorbate, have little effect on the PTM-TC spin probe signal (23). This specificity, along with the relatively sharp and distinct single-line ESR spectrum of the spin probe, also raises the possibility of one-dimensional (1D) high-resolution imaging. We implemented this methodology in a test case of superoxide generated in *Arabidopsis thaliana* plants after injury of the apical seedling area. Measurements were made at the whole plant level and on a more distal root tip region. We developed a novel (to our knowledge) small imaging resonator, a specialized sample holder, and sample preparation procedures to support the measurement of these challenging biological samples.

MATERIALS AND METHODS

Plant materials

Wild-type *A. thaliana* (ecotype Colombia) was used in this research. Seeds of *A. thaliana* were surface-sterilized with 6% sodium hypochlorite and 0.02% triton X-100 for 1 min. They were then transferred to 75% ethanol with 1.5% sodium hypochlorite and 0.02% triton X-100 for an additional 1-min wash. The seeds were then dried and sown in round Petri dishes containing half-strength Murashige-Skoog medium (26) in 0.8% agar. The plates were placed vertically in a growth chamber at 22°C under a 16-h photoperiod and ~50 μmol m^{-2} s^{-1} of light intensity. The plants in the experiments were 4–6 days old, with a typical length of ~20–30 mm and root diameter of ~0.2–0.4 mm.

ESR spin probes

The ESR spin probe, PTM-TC (Fig. 1 *a*) (23), was prepared in a 1-mM water solution and sonicated for 5 min. The solubility of this spin probe in open-air distilled water is slightly less than 1 mM; sonication expedites the solution preparation process and ensures solution saturation. The stable free radical PD-TEMPONE ^{15}N was 4-Oxo-2,2,6,6-tetramethylpiperidine-d_{16},1-^{15}N-1-oxyl, TEMPONE-d_{16},1-^{15}N obtained from Aldrich (St. Louis, MO) and prepared in a 1-mM water solution that served as a reference signal in some of the ESR measurements.

Sample preparation

The *A. thaliana* plants were gently lifted from the agar with the use of fine tweezers and rinsed twice in water. The whole plant was immersed in 100 μl of the PTM-TC solution for an incubation period of 30 min in the dark. Upon removal from the solution, the seedlings showed a very light red tan stain (the PTM-TC solution is red). They were washed in water for 15 s to remove the excess probe and then used immediately.

ESR system

All ESR experiments were carried out with a Bruker EMX continuous-wave (CW) system (Bruker Biospin, GmbH Rheinstetten, Germany) operating at an X-band frequency range (~9.3 GHz). Experiments involving measurements of whole plants were conducted with the original Bruker rectangular cavity (ER-4119HS). Experiments focusing on parts of the roots and 1D imaging experiments were performed with an in-house-built imaging dielectric resonator (DR; see below) that was attached to the Bruker system's microwave bridge, replacing the original cavity.

Imaging resonator and sample holder

The measurements and 1D imaging of the distal root tip region in the plant were carried out with an in-house-made imaging resonator, depicted in Fig. 2. The DR, located at the center of the apparatus, is made of a high-permittivity ($\varepsilon = 35$) ceramic material (3500 series from Trans-Tech, Adamstown, MD) machined to the following dimensions: 5.84 mm o.d., 2.1 mm i.d., and 2.68 mm high. The resonance frequency was measured as ~9.4 GHz with a quality factor (Q) of ~1500. The resonator is glued to a Rexolite holder and placed in a cylindrical, solid brass shield (12 mm i.d.). It focuses the microwave magnetic field on a relatively small volume at its center (see Fig. 2 *e*), thereby increasing the filling factor (27) that contributes to the sensitivity of the measurement of small, thin root samples (as described above). This compact resonator's geometry also makes it possible to place the gradient coils relatively close to the imaged object, thereby increasing their effectiveness for a given current drive. A pair of modulation coils and a set of 1D gradient coils are added to the structure (not shown in Fig. 2) to provide static field modulation (as required for CW ESR) and gradient encoding along the z axis of the imaging resonator, respectively. The gradient coils' typical electrical parameters are as follows: resistance of 1 Ω, inductance of 5 μH, and gradient efficiency of 0.36 T/m·A. The gradient coils are placed on a cylinder with a diameter of 10 mm around the resonator. They are driven by a current-controlled regulated power supply (E3640A from Agilent, Santa, Clara, CA) that can deliver 3 Å to the coils. The probe's interfaces to the microwave bridge (WR-90 waveguide) and the Bruker modulation source (BNC twinax

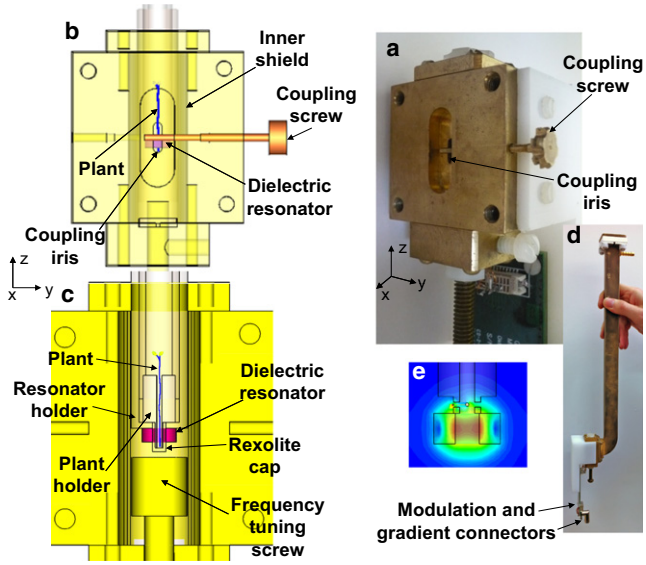

FIGURE 2 The imaging resonator for small plants that was developed in this work. (*a*) Isometric picture of the apparatus showing the coupling screw and coupling iris, when the waveguide transmission line (which is connected to the Bruker bridge on the other side) is disconnected. (*b*) A transparent view along the x axis, showing the position of the coupling screw with respect to the DR. The DR can be moved slightly (~1 mm) up and down to optimize coupling. The coupling screw is 1 mm in diameter, and the iris is 2 mm wide and 6 mm long. The larger depression between the waveguide and the iris has a width of 8 mm and height of 23 mm. (*c*) Cross section of the imaging probe in the central yz plane. (*d*) A broader view of the apparatus. (*e*) The distribution of the microwave magnetic field in the resonator's yz plane (calculated with finite element software; CST Microwave Studio).

connector) are identical to those of the original Bruker rectangular cavity (see Fig. 2, *c* and *d*). Iris matching is controlled manually by means of the coupling screw (Fig. 2 *a*).

We compared the sensitivity of the new imaging resonator with that of the Bruker cavity by measuring the ESR signal of a capillary tube (0.5-mm i.d.) filled with a 1-mM PTM-TC water solution. The use of a thin tube does not degrade much the quality factor, Q, of the Bruker cavity (Q = ~2000 with the tube) or the DR (Q = ~1400 with the tube). Fig. 3 *a* shows the ESR signal for the same tube in both resonators under the same modulation conditions (modulation amplitude and frequency = 0.7 G and 20 kHz, respectively). Microwave power was adjusted in the two measurements to obtain a maximal signal just below saturation condition (~8 mW for the Bruker cavity and ~0.7 mW for the DR). The signal in the DR is broader due to magnetic impurities in the brass and aluminum material from which it is made. Despite this broadening, it is evident that the signal is stronger than the one obtained from the Bruker cavity. Furthermore, it should be noted that for imaging applications in small, elongated biological samples, we are interested in the signal per unit of length and not in the total signal of the sample in the resonator. Thus, because the Bruker cavity is 23.5 mm long and the DR is ~4 mm long (note that the fields extend beyond the z axis of the DR; Fig. 2 *e*), it can be calculated that the DR is ~13.2 times more sensitive per unit of length. In addition to the whole-tube measurements, we carried out 1D imaging experiments with the same test sample. A typical result is shown in Fig. 3 *b*. In this case, the current in the gradient coils is 0.6 A, and it generates a gradient of ~0.21 T/m. Hence, the available resolution with gradient G_z can be calculated by the expression (28):

$$\Delta z = \frac{2\Delta B_{1/2}}{G_z} \quad (1)$$

where $\Delta B_{1/2}$ is the peak-to-peak linewidth of the ESR signal (~0.11 mT in the imaging resonator), leading to Δz = 1 mm. A deconvolution process (see below) further enhances the resolution by a factor of up to 2, so that a 1D image resolution of ~0.5 mm can be obtained with this relatively modest current. Higher currents can be supported but tend to create some drifts in the resonator's resonance frequency. This problem may be resolved in future designs by more efficient heat removal.

To facilitate the handling of samples with 200- to 400-μm-thick roots, which are very fragile and delicate, we developed a special sample holder that positions the root at the center of the resonator and protects it. In addition to their tensile weakness, these roots also tend to desiccate rapidly in the open air. The DR, however, has to maintain a high Q of at least 800–1000 to facilitate reasonable measurement conditions for the Bruker system. If the Q-value drops below these values, coupling and frequency locking on the resonator frequency becomes a problem. Because the presence of water can degrade Q significantly, the root cannot be placed in a completely aqueous environment. To meet all of these requirements, we designed the plant holder shown in Figs. 2 and 4 as a Rexolite cylinder with an o.d. of 5.6 mm, i.d. of 1.4 mm, and height of 8 mm, sliced in half. Rexolite exhibits low microwave losses and good machinability, and has a rather low dielectric constant that has a minimal effect on the resonator mode. Two halves of a vertically sliced capillary glass tube with 1.4 mm o.d. and 1 mm i.d. were glued to the Rexolite parts. These tube halves extend ~6 mm beyond the Rexolite cylinder (total height of 14 mm for the plant holder). During the sample preparation process, the plant is placed on one half of this structure with a minimal amount of water and then encapsulated by the other half. To avoid dehydration, we later placed a Rexolite cap (2.1-mm-o.d., 1.5-mm-i.d. tube, sealed on one side) on the bottom, thin part of this holder (Fig. 2 *b*). This sample preparation and holding scheme proved to be simple and capable of maintaining root hydration for the measurements.

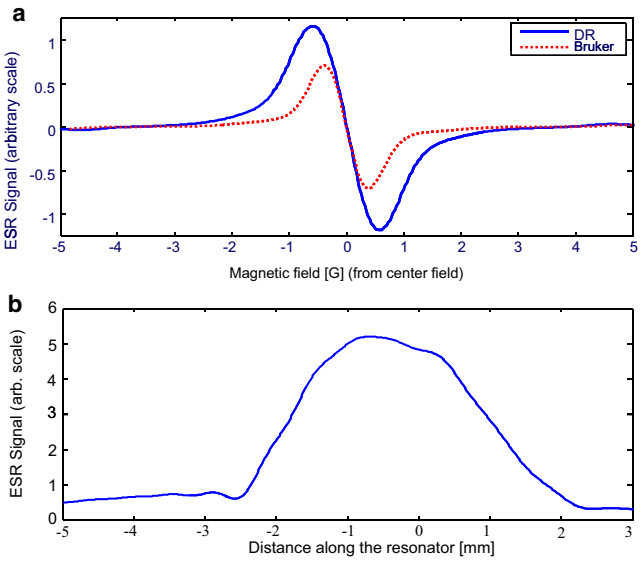

FIGURE 3 (*a*) ESR signal from a test sample of 1-mM PTM-TC water solution in a thin capillary tube as measured in the new DR (*solid line*) and Bruker (*dashed line*) cavity. (*b*) 1D ESR image of the sample placed in the imaging DR. The results shown were obtained after deconvolution of the original derivative ESR spectrum with the gradient by the spectrum without such gradient. The signal is slightly asymmetric with respect to the resonator's center, probably due to the nonsymmetric position of the coupling screw (Fig. 2), which is not exactly at the center of the resonator.

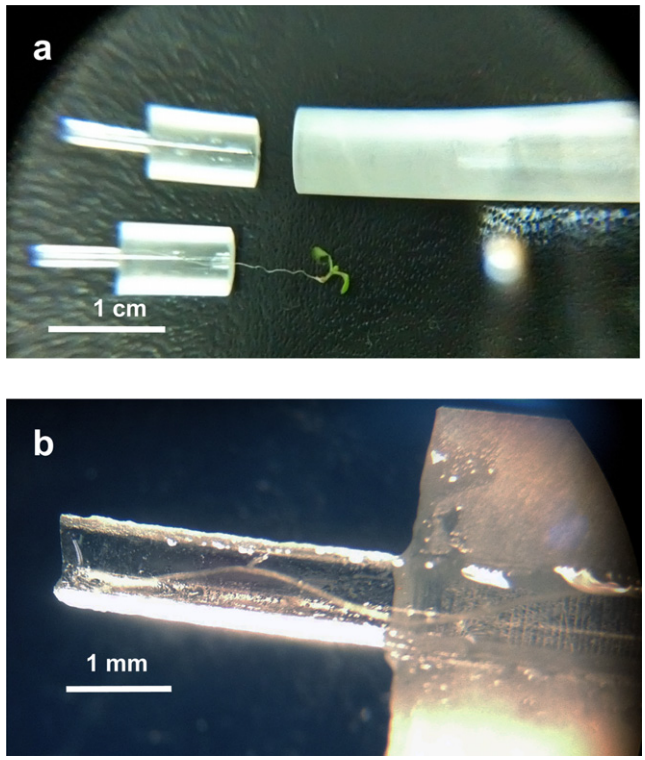

FIGURE 4 Photograph of the special sample holder for plants developed in this work. (*a*) A wide view of the two halves of the sample holder, as described in the text. The two halves with the plant are inserted into the holding tube shown on the right. (*b*) Close-up view of the sample holder's lower section, where the bottom part of the root is placed. This thinner part is then covered with a small Rexolite cap and placed inside the resonator's effective volume.

Data analysis

The ESR signal amplitude in the whole-plant measurements (carried out with the conventional Bruker rectangular cavity) was taken as the peak-to-peak CW spectrum of the PTM-TC radical divided by the peak-to-peak signal of a reference 1-mM sample of PD-TEMPONE ^{15}N (Fig. 1). We obtained the 1D spin probe concentration profiles by measuring the CW ESR spectrum with and without a static gradient along the z axis of the imaging resonator and then deconvoluting the former measurement using the latter as a deconvolution kernel (28).

RESULTS

Whole-plant measurements

In the first set of experiments, we examined the penetration of the spin probe into control plants and the maintenance of signal integrity over time. The plants were incubated in a 1-mM PTM-TC water solution (see "ESR spin probes" above) and then measured in a standard 4-mm-o.d. ESR test tube together with a small capillary of 1-mM PD-TEMPONE ^{15}N water solution. Typical representative results for these types of experiments are shown in Fig. 5. It is clear that the signal from the spin probe in the plant showed no apparent change within a 30-min time frame. These experiments were repeated with more than 10 plants and showed similar results up to a time frame of 60 min. Removing the plant and then repeating the measurements with the residual water left in the ESR tube still resulted in some small signal, meaning that the spin probe can diffuse out of the plant. This was verified by other experiments in which the plant was first incubated, measured to give a good signal, and then left for 30 min in water, which resulted in a large loss of signal from the plant (~50–70%) accompanied by loss of the light-red tan color indicative of the presence of PTM-TC. The loss of spin probe is consistent with its apoplastic location. In view of this phenomenon, and to optimize spin probe detection, care was taken to insert the plants into the tube with minimal residual water. This also made it possible to minimize the reduction in the Q of the resonator (see "Imaging resonator and sample holder" above). In some cases, however, the plant was inserted without sufficient water, resulting in partial dehydration and the generation of solid radical aggregates with a relatively broad ESR spectrum (spectral wings in Fig. 5, also apparent in Figs. 6 *a* and 7 *a*). The presence of solid radical aggregates in the tube does not interfere with the measurement; however, they cannot participate effectively in the superoxide reactions. Thus, we adopted ~40 min as the nominal total experiment time to minimize signal loss and maintain proper hydration of the tissue. In summary, having too much water is good for root viability but bad for the resonator Q and the measurement procedure. This is because the superoxide cannot affect the spin probe that diffuses outside the plant, and therefore, in such cases, it appears as if there is almost no superoxide burst. On the other hand, having some aggregates present in the solution or in the plant is fine as long as they do not dominate the ESR signal and do not continue to aggregate during measurement (as a result of dehydration; see also Discussion section). Thus, the most favorable preparation is just to leave the plant with the small, thin layer of water that attaches to it after rinsing.

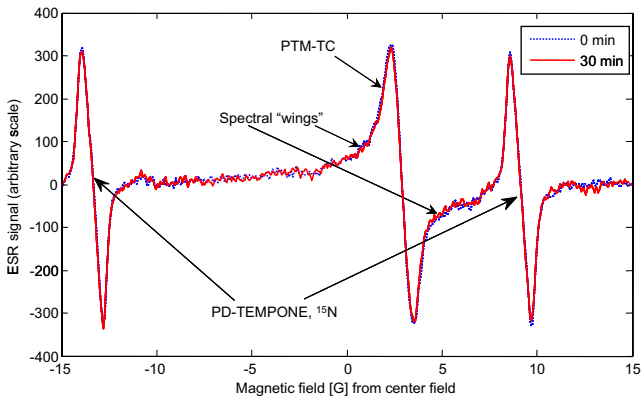

FIGURE 5 CW ESR signal of a whole plant with PTM-TC measured in the rectangular Bruker cavity at two times. (0 min – *dashed line*, 30 min – *solid line*). The PD-TEMPONE ^{15}N signal is used as a reference. Measurement conditions: center field 0.3365 Tesla, modulation amplitude 1.3 G, modulation frequency 20 kHz, number of points 512, time constant 42 ms.

Next, we examined the PTM-TC signal in the plant as a response to injury. Wounding results in the rapid generation of superoxide as measured by fluorescence probes (29). We first measured whole plants in the ESR tube as described above to establish the basal signal level. We removed the tube and injured the leaves by pressing them with a sharp object under a binocular microscope while they were still in the ESR tube. The ESR tube was then immediately placed back into the cavity for further measurements of the time-resolved ESR signal. Data were normalized to the signal of the reference PD-TEMPONE ^{15}N sample, to eliminate possible changes in the ESR signal due to the removal and the insertion of the ESR tube or other possible drifts in the system. Typical results for this type of experiment are shown in Fig. 6 *a* for an individual plant, and a summary of signal decays from 17 plants is presented in Fig. 6 *b*. It is clear that injury leads to a rapid decrease in spin-probe signal, and most of the loss in signal intensity occurs within 1 min of injury. Of importance, the signal due to solid radical aggregates (i.e., the wings in the spectrum) is pronounced but hardly changes during injury (Fig. 6 *a*) because it emanates from a probe that is out of the solution and does not participate efficiently in the reactions with the superoxide.

Root ESR measurements and 1D imaging

To assess the usefulness of the new imaging resonator and sample holder, we incubated individual plants in the spin probe solution and then measured them in the imaging resonator with and without a z-gradient. Subsequently, the

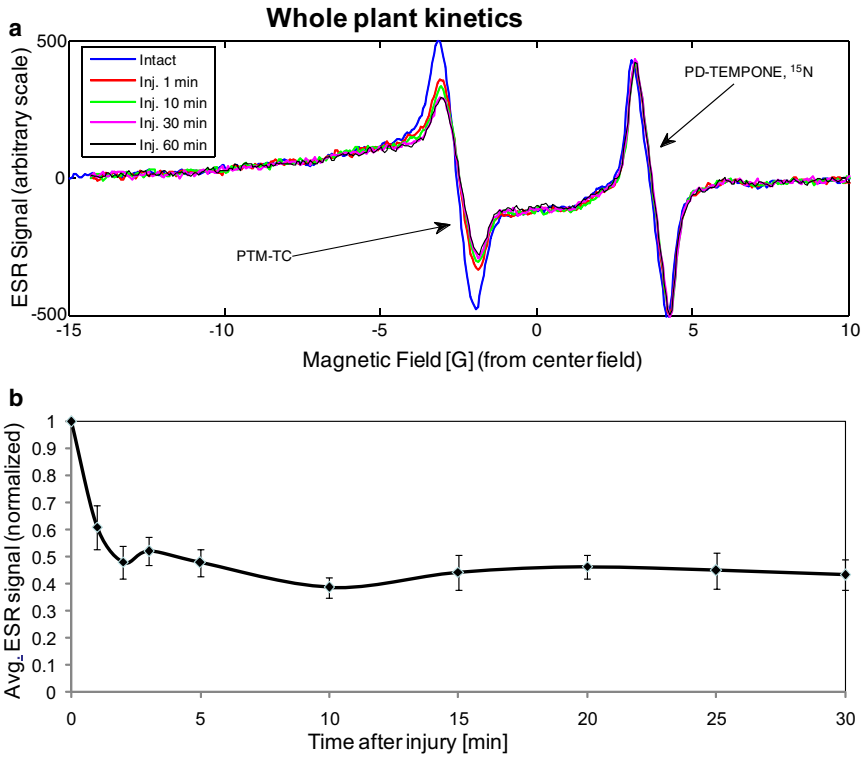

FIGURE 6 (*a*) Typical CW ESR signal of a whole plant with PTM-TC measured in the rectangular Bruker cavity as a function of time, before and after leaf injury. The PD-TEMPONE ^{15}N signal is used as a reference. Measurement conditions are the same as in Fig. 5. (*b*) Summary of CW ESR measurements carried out with 17 different plants, as a function of time after injury. The signal is normalized to the PD-TEMPONE ^{15}N reference and also to the initial signal before injury.

sample holder containing the plant was removed, and the plant was injured and measured again with and without a *z*-gradient in a time-resolved manner. In this experiment, the internal reference was omitted because it would have overlapped with the sample signal once the gradient was applied. Nevertheless, changes in the ESR signal due to removal and reinsertion of the sample were expected to be minimal because of the accurate machining of the resonator and the tightly fitted sample holder, and the fact that the injury was carried out without moving the distal parts of the plants on which measurements were done. We verified that omission of the reference was indeed possible by noting that multiple removal and reinsertion of the sample holder from and into the imaging resonator did not alter the signal intensity. Fig. 7 *a* shows the typical results of the ESR signal without gradient as a function of time after injury. This signal originates only from the lower ~4 mm of the root, which is inside the effective volume of the resonator (see Figs. 2 and 3). Again, Fig. 7 *a* shows that the aggregated spin probe (the broad signal wings in the spectrum) does not participate in the reaction with the superoxide. Fig. 7 *b* shows a summary of measurements from the distal part (without gradient) based on the measurements of eight plants. Fig. 8 *a* provides a typical 1D ESR image of the distal part of the root as a function of time after injury. These 1D ESR images were obtained with a *z*-gradient of 0.21 T/m and spectrum deconvolution process, as described above. The 1D image enables us to examine the kinetics in finer resolution, looking at three different positions in the root, as marked in Fig. 8 *a*. The normalized signals' reduction kinetics at these selected positions are presented in Fig. 8 *b* and show that the signal within the 4-mm root tip region is more rapidly reduced and to a lower relative level at positions 1 and 2 compared with position 3.

DISCUSSION

Obtaining accurate measurements of short-lived ROS, such as superoxide, in biological systems is a complicated and delicate task. ESR measurements employing spin traps are commonly considered to be the most accurate and reliable method for measuring ROS. However, solvent compatibility with living tissue, high concentrations of probe (well above 10 mM), lack of sensitivity, and a broad spectrum (>10 G) that severely limits imaging options can be major limitations in the practical in vivo use of the ESR spin-trapping method. Here, we made use of a stable spin probe (PTM-TC) rather than spin traps. The spin probe can be administered in a relatively low concentration (~1 mM) in water solution and has a strong and relatively sharp signal (~1 G wide). These factors make the spin probe more compatible with biological samples and more suitable for ESR imaging. We have shown the potential capability of this approach to monitor superoxide at sufficient spatial and temporal resolutions. Although PTM-TC identification of superoxide is not spectroscopic, as it is with spin traps, its reaction embodies an exceptionally high second-order reaction rate constant with superoxide that is about one-fourth that of SOD. Furthermore, PTM-TC was shown to display high specificity to superoxide (23), providing confidence in the quantitative

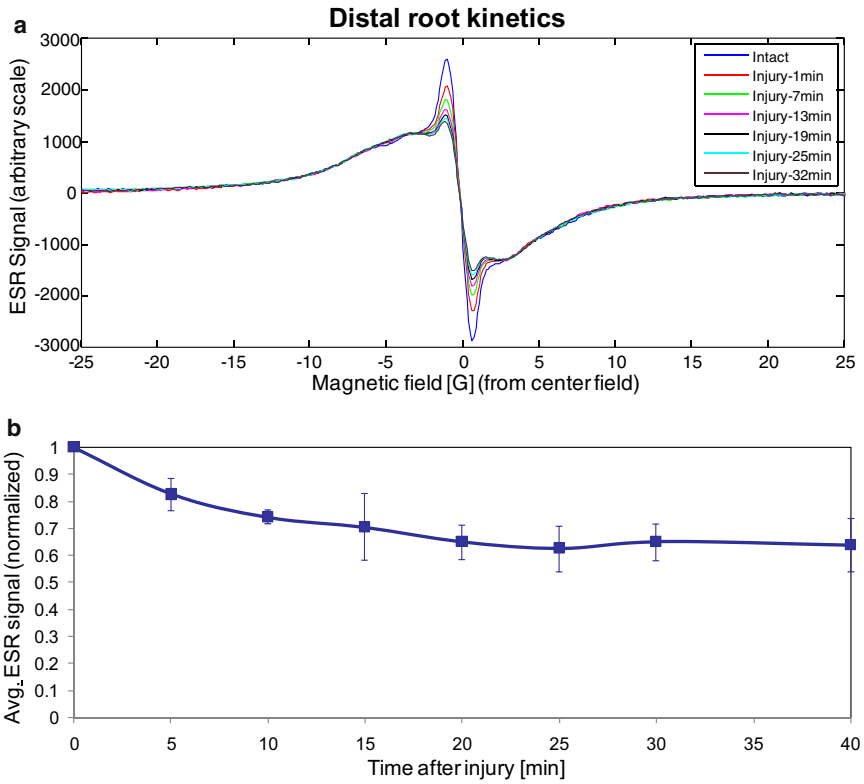

FIGURE 7 (*a*) Typical CW ESR signal of the ~4 mm distal part of the plant with PTM-TC measured in the special imaging resonator as a function of time, before and after leaf injury. Measurement conditions are the same as in Fig. 5. (*b*) Summary of several CW ESR measurements carried out with eight different plants, as a function of time after injury. The signal is normalized to the initial signal before injury.

nature of this method. It should be noted that in many spin traps and fluorescence probes, hydroxyl radicals may interfere with the superoxide signal. It is difficult to make a clear-cut claim about this issue as regards the in vivo situation; however, our in vitro experiments using Fenton chemistry showed a lack of specific reactivity of OH toward the trityl radicals (23). Thus, because of the high reactivity of hydroxyl radicals with anything that comes across within a few angstroms, they decay so rapidly that there may not be sufficient concentration in vivo to react with our spin

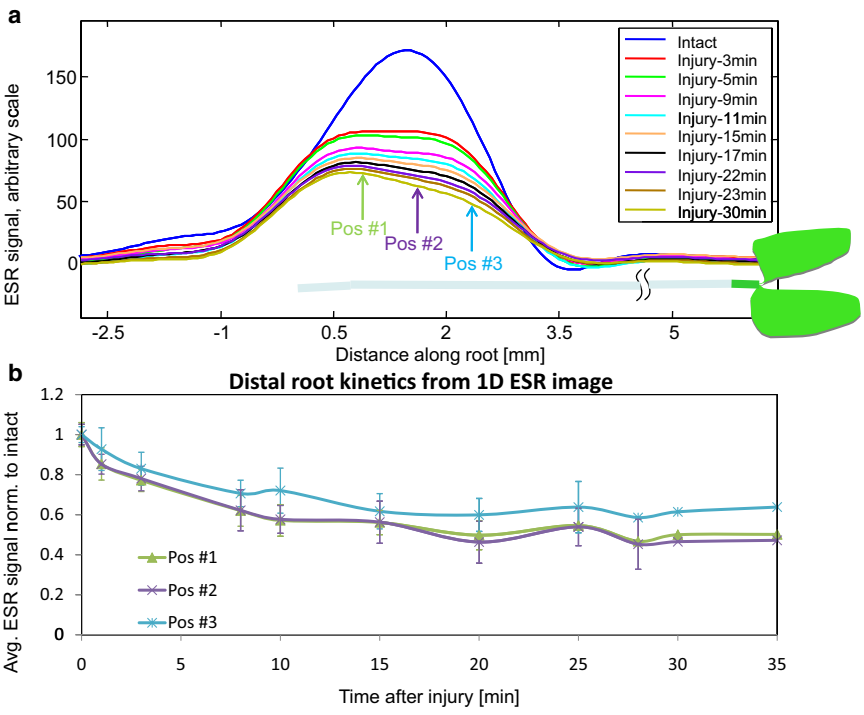

FIGURE 8 (*a*) Typical 1D ESR images of the ~4 mm distal part of the root as a function of time, as measured in the special imaging resonator. (*b*) Summary of the kinetic responses measured in eight plants from the 1D ESR time-resolved images, in three different positions (marked in panel *a*) along the distal part of the root.

probe. PTM-TC is negatively charged in its soluble state and cannot efficiently penetrate the plant's cell membrane. However, as shown in Figs. 6–8 for plant injury response, although the PTM-TC spin probe is not cell-permeable, it does facilitate the readout of superoxide. These superoxides are either produced at the membrane or reach the plant's apoplast region from internal sources. The observation of relatively free spin-probe diffusion in and out of the plant, as mentioned in the Results section, also supports this conclusion. This is in agreement with previous work in which we showed that superoxides originating from plant NADPH oxidases can be found in both intra- and extracellular locations (30,31).

Injury in plant leaves is known to propagate superoxide rapidly in both damaged and undamaged systemic leaf tissue (32). Indirect measurements based on gene promoters that are sensitive to cellular redox state fusions with the luciferase reporter showed rapid propagation within minutes from leaf to leaf (7). Our results from whole plants, as described in Fig. 6, clearly show the ability of the method to provide details of the superoxide burst in the plant after injury. The time resolution of our measurements is ~1 min due to limitations in the injury procedure and spectrum acquisition time in the Bruker machine. This time resolution is on the edge of being sufficient to monitor signal decay in the whole plant, especially in the initial period after injury. It can be improved in the future by the use of an in-house-made spectrometer and resonator that would enable faster acquisition times by acquiring spectra with fewer field points (much less than the minimal 512 points provided by our Bruker EMX system software) and with small and fast-response field-scan coils integral to the imaging probe. The new resonator setup should also allow one to perform the injury procedure while the plant is in the resonator. The concentration of the spin probe in the plant can be estimated to be ~0.5 mM based on the estimated volume of the plant and its typical signal (e.g., Fig. 5) versus the reference 1-mM sample we used in Fig. 3. On the basis of this information and the second-order reaction rate constant with superoxide mentioned above, we can place a lower limit of at least $\sim 2\times10^{-11}$ M for the steady-state superoxide concentration after injury. In practice, given SOD reactions that probably operate in parallel and our limited time resolution, one could expect this concentration to be larger. Future experiments with better time resolution and a proper disabling of SOD activity will be able to provide much more accurate results in this respect.

The development of a new compact imaging resonator with relatively high 1D imaging resolution capabilities, together with a unique sample holder and sample handling procedure, enabled us to inspect in more detail the spatial and temporal development of the superoxide signal. Even without the use of gradients, the resonator measurements show for the first time (to our knowledge) superoxide generation in the distal part of a root after leaf wounding. As is evident in Fig. 7, superoxide is generated in a delayed response relative to the whole plant signal, and its steady-state concentration seems to be lower in the ~4-mm distal part than when averaged over the entire plant. (However, as mentioned above, accurate results for superoxide concentration would also require disabling the SOD activity.) The results in Figs. 7 *a* and 8 *a* show an ~50% signal reduction within 1–3 min of wounding. Based on the distance from the leaf and the root length (3 cm), we conclude that the wound signal is transmitted in the roots at a rate of at least 1–3 cm/min. This value in the root is slightly lower than the number reported for the transmission of redox signal in the stem (8.4 cm/min) (7). Further experiments with an improved resonator setup (see below) would provide more-precise kinetic measurements. Thus, no conclusions about tissue-specific differences can be drawn at present.

As noted above, many of the ESR spectra we acquired showed broad wings due to spin-probe aggregation. The ratio of soluble-to-aggregated signal can vary from root to root and is probably dependent on sample preparation conditions, because these young and gentle roots tend to dehydrate very rapidly in the open air. Improvements in sample preparation (e.g., keeping it under moist conditions at all times), should minimize this effect. Of importance, as shown above, the aggregated radical is inert to the superoxide and therefore does not participate in or interfere with the measurement procedure (it simply observes it from the side). Thus, as long as not too much of the signal is lost due to aggregation during sample preparation, there is no real harm in this effect. However, further dehydration, leading to additional aggregation during the actual measurements, must be eliminated because it can be wrongly interpreted as a loss of signal due to superoxide reactions. This can be achieved by ensuring some plant hydration, efficient sample sealing, and limiting the measurement time to ~40 min, as mentioned above.

Further insights into spatial and temporal ESR signal variations along the root are provided by the 1D ESR images of the distal part, shown in Fig. 8 *a*. As noted above, the spatial resolution for this type of measurement is ~0.5 mm, which is just enough to acquire useful information from such a short plant section (~4 mm). It would be very difficult to obtain measurements with such resolution using the commercial Bruker cavity, which is much larger. Indeed, the simple addition of gradient coils to this cavity would not suffice to improve resolution because the sensitivity per unit of length is an order of magnitude smaller than that achieved by the resonator configuration employed here. The main novelty of our finding is in the direct recording of superoxide release in the roots after injury in the apical parts. The results of Fig. 8 *b* show that the distal parts of the imaged 4-mm section accumulate slightly more superoxide than the proximal part. The reason for this is unknown and may indicate that processes that generate superoxide are more enriched near the root tip, where less-mature root cells are located.

The 1D ESR image profiles shown in Fig. 8 *a* are generated by a mathematical process of deconvolution using the spectrum with and without the gradient, and therefore should be viewed with caution. Although the mathematical process in itself is reliable and well-established (28), during protracted measurements (>30 min), the ESR spectrum (without gradient) changes not only in magnitude but also in shape. In this work, we could not sample the ESR spectrum with and without gradient at the same time. This means that deconvolution is carried out with a gradient-free spectrum that may differ from the one relevant to the time in which the ESR spectrum was measured with the gradient. This could distort the deconvoluted 1D image and introduce artifacts. Another problem is that the deconvolution process assumes that the spectrum is similar throughout the sample and only the spin-probe concentration changes. This is not necessarily the case in our samples, because the aggregated parts may be located at some specific point in the root, i.e., the partition between the free and the aggregated spin probe may differ throughout the root. The ultimate solution to these problems is to employ a faster imaging algorithm for spectral-spatial imaging, which provides a spatially resolved ESR spectrum (33,34).

We are currently constructing a more advanced resonator that should be able to look at an entire root by combining several DRs stacked one on top of the other (35,36). The future incorporation of fast spectral-spatial imaging capabilities will also help investigators extract artifact-free spectral-spatial information that can be analyzed in a quantitative manner and may shed light on superoxide signaling in plants. Another challenge will be to develop new spin probes with membrane permeability and cellular retention capability. The progress shown here makes the development of such probes worthwhile and inviting.

This work was partially supported by grant 213/09 from the Israeli Science Foundation, grant 2005258 from the Binational Science Foundation, and grant 201665 from the European Research Council.

REFERENCES

1. Buetler, T. M., A. Krauskopf, and U. T. Ruegg. 2004. Role of superoxide as a signaling molecule. *News Physiol. Sci.* 19:120–123.
2. Dunand, C., M. Crèvecoeur, and C. Penel. 2007. Distribution of superoxide and hydrogen peroxide in *Arabidopsis* root and their influence on root development: possible interaction with peroxidases. *New Phytol.* 174:332–341.
3. Tsukagoshi, H., W. Busch, and P. N. Benfey. 2010. Transcriptional regulation of ROS controls transition from proliferation to differentiation in the root. *Cell.* 143:606–616.
4. Simon-Plas, F., T. Elmayan, and J.-P. Blein. 2002. The plasma membrane oxidase NtrbohD is responsible for AOS production in elicited tobacco cells. *Plant J.* 31:137–147.
5. Bolwell, G. P., V. S. Butt, …, A. Zimmerlin. 1995. The origin of the oxidative burst in plants. *Free Radic. Res.* 23:517–532.
6. Bolwell, G. P., D. R. Davies, …, T. M. Murphy. 1998. Comparative biochemistry of the oxidative burst produced by rose and french bean cells reveals two distinct mechanisms. *Plant Physiol.* 116:1379–1385.
7. Miller, G., K. Schlauch, …, R. Mittler. 2009. The plant NADPH oxidase RBOHD mediates rapid systemic signaling in response to diverse stimuli. *Sci. Signal.* 2:ra45.
8. Miller, G., N. Suzuki, …, R. Mittler. 2010. Reactive oxygen species homeostasis and signalling during drought and salinity stresses. *Plant Cell Environ.* 33:453–467.
9. Gardner, P. R. 2002. Aconitase: sensitive target and measure of superoxide. *Methods Enzymol.* 349:9–23.
10. Armstrong, J. S., and M. Whiteman. 2007. Measurement of reactive oxygen species in cells and mitochondria. *Methods Cell Biol.* 80:355–377.
11. Fridovich, I. 1997. Superoxide anion radical ($O_2^{-\cdot}$), superoxide dismutases, and related matters. *J. Biol. Chem.* 272:18515–18517.
12. Gomes, A., E. Fernandes, and J. L. F. C. Lima. 2005. Fluorescence probes used for detection of reactive oxygen species. *J. Biochem. Biophys. Methods.* 65:45–80.
13. Tarpey, M. M., D. A. Wink, and M. B. Grisham. 2004. Methods for detection of reactive metabolites of oxygen and nitrogen: in vitro and in vivo considerations. *Am. J. Physiol. Regul. Integr. Comp. Physiol.* 286:R431–R444.
14. Jambunathan, N. 2010. Determination and detection of reactive oxygen species (ROS), lipid peroxidation, and electrolyte leakage in plants. *Methods Mol. Biol.* 639:292–298.
15. Liszkay, A., E. van der Zalm, and P. Schopfer. 2004. Production of reactive oxygen intermediates (O(2)(.-), H(2)O(2), and (.)OH) by maize roots and their role in wall loosening and elongation growth. *Plant Physiol.* 136:3114–3123, discussion 3001.
16. Georgiou, C. D., I. Papapostolou, and K. Grintzalis. 2008. Superoxide radical detection in cells, tissues, organisms (animals, plants, insects, microorganisms) and soils. *Nat. Protoc.* 3:1679–1692.
17. Wang, W., H. Q. Fang, …, H. Cheng. 2008. Superoxide flashes in single mitochondria. *Cell.* 134:279–290.
18. Khan, N., C. M. Wilmot, …, H. M. Swartz. 2003. Spin traps: in vitro toxicity and stability of radical adducts. *Free Radic. Biol. Med.* 34:1473–1481.
19. Zhao, H. T., J. Joseph, …, B. Kalyanaraman. 2001. Synthesis and biochemical applications of a solid cyclic nitrone spin trap: a relatively superior trap for detecting superoxide anions and glutathiyl radicals. *Free Radic. Biol. Med.* 31:599–606.
20. Vylegzhanina, N. N., L. K. Gordon, …, O. P. Kolesnikov. 2001. Superoxide production as a stress response of wounded root cells: ESR spin-trap and acceptor methods. *Appl. Magn. Reson.* 21:63–70.
21. Renew, S., E. Heyno, …, A. Liszkay. 2005. Sensitive detection and localization of hydroxyl radical production in cucumber roots and *Arabidopsis* seedlings by spin trapping electron paramagnetic resonance spectroscopy. *Plant J.* 44:342–347.
22. Likhtenshtein, G. I. 2009. Novel fluorescent methods for biotechnological and biomedical sensoring: assessing antioxidants, reactive radicals, NO dynamics, immunoassay, and biomembranes fluidity. *Appl. Biochem. Biotechnol.* 152:135–155.
23. Kutala, V. K., F. A. Villamena, …, P. Kuppusamy. 2008. Reactivity of superoxide anion radical with a perchlorotriphenylmethyl (trityl) radical. *J. Phys. Chem. B.* 112:158–167.
24. Swartz, H. M., M. Sentjurc, and P. D. Morse, 2nd. 1986. Cellular metabolism of water-soluble nitroxides: effect on rate of reduction of cell/nitroxide ratio, oxygen concentrations and permeability of nitroxides. *Biochim. Biophys. Acta.* 888:82–90.
25. Rizzi, C., A. Samouilov, …, P. Kuppusamy. 2003. Application of a trityl-based radical probe for measuring superoxide. *Free Radic. Biol. Med.* 35:1608–1618.
26. Murashige, T., and F. Skoog. 1962. A revised medium for rapid growth and bio assays with tobacco tissue cultures. *Physiol. Plant.* 15:473.
27. Poole, C. P. 1983. Electron Spin Resonance: A Comprehensive Treatise on Experimental Techniques. Wiley, New York.
28. Eaton, G. R., S. S. Eaton, and K. Ohno. 1991. EPR Imaging and In Vivo EPR. CRC Press, Boca Raton.

29. Sagi, M., and R. Fluhr. 2006. Production of reactive oxygen species by plant NADPH oxidases. *Plant Physiol.* 141:336–340.

30. Ashtamker, C., V. Kiss, …, R. Fluhr. 2007. Diverse subcellular locations of cryptogein-induced reactive oxygen species production in tobacco Bright Yellow-2 cells. *Plant Physiol.* 143:1817–1826.

31. Sagi, M., and R. Fluhr. 2001. Superoxide production by plant homologues of the gp91(phox) NADPH oxidase. Modulation of activity by calcium and by tobacco mosaic virus infection. *Plant Physiol.* 126:1281–1290.

32. Sagi, M., O. Davydov, …, R. Fluhr. 2004. Plant respiratory burst oxidase homologs impinge on wound responsiveness and development in *Lycopersicon esculentum*. *Plant Cell.* 16:616–628.

33. Eaton, G. R., S. S. Eaton, and M. M. Maltempo. 1989. Three approaches to spectral spatial EPR imaging. *Appl. Radiat. Isot.* 40:1227–1231.

34. Blank, A., R. Halevy, …, P. Kuppusamy. 2010. ESR micro-imaging of LiNc-BuO crystals in PDMS: spatial and spectral grain distribution. *J. Magn. Reson.* 203:150–155.

35. Jaworski, M., A. Sienkiewicz, and C. P. Scholes. 1997. Double-stacked dielectric resonator for sensitive EPR measurements. *J. Magn. Reson.* 124:87–96.

36. Karp, A., H. J. Shaw, and D. K. Winslow. 1968. Circuit properties of microwave dielectric resonators. *IEEE Trans. Microwave Theory Tech.* 16:818–828.